Superparamagnetic lipid-based hybrid nanosystems for drug delivery

E. Millart, S. Lesieur, V. Faivre

Expert Opinion on Drug Delivery

ISSN: 1742-5247 (Print) 1744-7593 (Online) Journal homepage: http://www.tandfonline.com/loi/iedd20

Superparamagnetic lipid-based hybrid nanosystems for drug delivery

E. Millart, S. Lesieur & V. Faivre

To cite this article: E. Millart, S. Lesieur & V. Faivre (2018) Superparamagnetic lipid-based hybrid nanosystems for drug delivery, Expert Opinion on Drug Delivery, 15:5, 523-540, DOI: 10.1080/17425247.2018.1453804

To link to this article: https://doi.org/10.1080/17425247.2018.1453804

Accepted author version posted online: 15 Mar 2018.
Published online: 29 Mar 2018.

EXPERT OPINION ON DRUG DELIVERY, 2018
VOL. 15, NO. 5, 523–540
https://doi.org/10.1080/17425247.2018.1453804

Taylor & Francis
Taylor & Francis Group

REVIEW

Superparamagnetic lipid-based hybrid nanosystems for drug delivery

E. Millart, S. Lesieur and V. Faivre

Institut Galien Paris-Sud, CNRS, Univ. Paris-Sud, Université Paris-Saclay, Châtenay-Malabry, France

ABSTRACT

Introduction: The development of multifunctional drug carriers provides many opportunities in the field of drug delivery. Among them, carriers loaded with both drug and superparamagnetic iron oxide nanoparticles would allow the combination of chemotherapy with the possibility of monitoring or controlling the distribution of the nanocarrier in the body, triggering drug release and/or applying a synergistic hyperthermia treatment.

Areas covered: The present review covers biocompatible lipid-based nanotechnologies that have been employed to co-encapsulate drug and iron oxide. Depending on their physico-chemical properties, lipids are able to generate monophasic lipophilic nanodispersions or more complex structures containing both lipidic and aqueous domains. This review describes the rationale behind these nanoobjects and how they can be prepared.

Expert opinion: This review focuses on the co-encapsulation aspects of these hybrid systems and discusses in particular the possible heterogeneities in drug-to-iron oxide ratio and the difficulties that could be encountered in the construction of these biocompatible multifunctional drug carriers.

ARTICLE HISTORY
Received 31 May 2017
Accepted 14 March 2018

KEYWORDS
Cubosomes; iron oxide; ISAsomes; liposome; nanoemulsions; NLC; SLN; SPION

1. Introduction

Superparamagnetic iron oxide nanoparticles (SPION) are single crystals of iron oxide (nanocrystals) which are often coated with inorganic or organic materials of varying chemical properties that act mainly as stabilizers of the colloidal state. The dispersion of SPION within a carrier fluid such as water or organic solvent yields a colloidal suspension called ferrofluid. It has long been a scientific and technological challenge to synthesize these systems and control their size distribution and shape. As well as conventional reaction processes based on redox-assisted precipitation of iron salts [1], more recent strategies for obtaining calibrated iron oxide crystals in the nanometer range have emerged over the last decade, including solvothermal, biomineralization or surfactant-assisted routes [2,3]. At the same time, surface modification or functionalization through covalent or non-covalent binding of molecules or macromolecules has been extensively developed as a means of modulating the dispersibility of the nanocrystals in different liquid phases while preserving a stable suspension state therein. The most significant example concerns biomedical applications for which stability in physiological fluids is essential. In this respect, simple surface coating of SPION has been intentionally replaced or complemented by hierarchical formulations leading to their incorporation/encapsulation within protective and possibly functional, reservoir systems while preserving or even enhancing their superparamagnetic behavior. The advantage of this approach is to allow the combination of SPION properties with other actions such as therapeutic activity through the co-encapsulation of drugs. The present review focuses on the latter aspect when lipid-based nanotechnology has been employed and tries to give an overview of the different types of application that can be envisaged for such multifunctional hybrid systems.

2. Superparamagnetic iron oxide nanoparticles (SPION)

2.1. Structure and magnetic properties

SPION used for biomedical applications often consist of two components, an iron oxide core and a hydrophilic or hydrophobic surface coating. The iron oxide core is nanometric and can be composed of magnetite (FeO, Fe_2O_3, or Fe_3O_4) and/or maghemite (γ-Fe_2O_3) usually in the single-crystal state. Maghemite, the ferromagnetic cubic form of Fe(III) oxide, is closely related to the structure of inverse spinel Fe_3O_4 but differs by the presence of vacancies distributed within the cation sublattice [4]. The magnetic properties present in some ferromagnetic materials are the result of aligned unpaired electron spins. In a non-magnetized ferromagnetic material, the magnetic moments of the magnetic domains (Weiss-domains) are aligned at short range, but at long range, the magnetic moments of adjacent domains are anti-aligned. Superparamagnetism occurs when the size of the crystals is smaller than that of ferromagnetic domains (0.03–0.05 µm) and as a result there is no magnetic remanence, unlike ferromagnetic materials [5]. Each crystal is then considered to be a fully magnetized single magnetic monodomain, and can be considered to be a monomagnet as a direct consequence of the spinel structure of the crystal, permitting strong magnetic coupling and consequently perfect alignment

CONTACT V. Faivre vincent.faivre@u-psud.fr

Article highlights

- Superparamagnetic iron oxide nanoparticles (SPION) can be used for magnetic resonance imaging, physical targeting, hyperthermia and/or temperature-triggered drug release.
- Depending on their physico-chemical properties, lipid-based components are able to generate monophasic or compartmented nanoscale assemblies that allow double incoporation of superparamagnetic nanomaterials and drugs.
- This review highlights the potential applications of magnetic-fluid-loaded lipid nanocarriers as multifunctional systems.
- The discussion has been focused on the limits of co-encapsulation and the strategies to guarantee the drug-to-SPION ratio.

This box summarizes key points contained in the article

of the individual magnetic spins. The temperature at which a particle becomes superparamagnetic is called the blocking temperature (T_B) and defined as:

$$T_B = \frac{KV}{k_B \ln\left(\frac{\tau_m}{\tau_0}\right)} \quad (1)$$

where K is the magnetic anisotropy constant, V is the volume of a nanoparticle, k_b is the Boltzmann constant, τ_m is the measurement time and τ_0 is a length of time, characteristic of the material, called the *attempt time* or *attempt period* [6]. When SPION are placed in an external magnetic field their moments align in the direction of the magnetic field. This ability to elicit substantial disturbances in the local magnetic field through large magnetic moments leads to a rapid dephasing of surrounding protons, generating a detectable change in the magnetic resonance signal. Thus, the imaging capability provided is not from the SPION themselves, but through their influence on longitudinal and transverse relaxation of the surrounding nuclei [7]. If desired, to complete this brief overview, more information on superparamagnetism is available in the literature [8,9].

2.2. Biocompatibility – biodegradability

Before SPION can be used *in vivo*, biocompatibility is a crucial factor that must be studied. Usually, SPION have a good biocompatibility profile [10,11] and their uptake by macrophages is not associated with cell activation. The extent of SPION biocompatibility depends mainly on the nature of the magnetic content, final NP size and the nature of the coating. Human tissues may contain iron or iron oxides in the form of hemosiderin, ferritin and transferrin. Normal liver contains approximately 0.2 mg of iron per gram and total human iron stores amount to 3500 mg. The total amount of iron oxide used in diagnostic imaging (50–200 mg Fe) is minor compared with the body's normal iron store. Chronic iron toxicity develops only after the liver iron concentration exceeds 4 mg Fe/g [12]. The particle size affects cellular uptake, biodistribution, and other pharmacokinetics. The size of iron oxide nanoparticles should be optimized to avoid rapid clearance by the body's immune system, and consequently to be accumulated sufficiently in the target tissue or organ. The optimal size range can differ depending on the shape, surface composition and charge [13] but it was reported that very small-sized nanoparticles (hydrodynamic diameter of <5–10 nm) are excreted renally [14] whereas medium-sized nanoparticles (30–150 nm) undergo a wide distribution to bone marrow, heart, kidney, and stomach [15]. Meanwhile, large particles with hydrodynamic diameter of >50–100 nm are easily taken up by phagocytes [16] and therefore accumulate rapidly in tissues such as the liver and spleen [17]. Interestingly, nanoparticles of 10–20 to 100–150 nm tend to accumulate in tumors through the enhanced permeability and retention (EPR) effect, because cancerous tissues generally combine fenestration of blood vessels with gaps of hundreds of nanometers in size [18,19] and poor lymphatic drainage. In order to prolong plasma half-life, amphiphilic coatings are the most efficient, extending the circulation time of the particulate from minutes to hours [20]. In addition to renal excretion, SPION are suggested to also be degraded and cleared from the body through the endogenous iron metabolic pathway [21]. The released iron is first metabolized in the liver and then either used in production of red blood cells or eliminated from body through the kidneys.

2.3. Applications (MRI, magnetophoric mobility, hyperthermia)

In addition to tissue density, tissue relaxation properties (T_i) contribute to image contrast in MRI. During the process of T_1 relaxation, protons reorient leading to the recovery of longitudinal magnetization. During the process of T_2 relaxation, protons dephase resulting in a decay of transverse magnetization. T_2* relaxation refers to decay of transverse magnetization caused by a combination of T_2 relaxation and magnetic field inhomogeneity. Superparamagnetic nanoparticles are most commonly used as contrast agents because of their negative enhancement effect on T_2- and T_2*-weighted sequences. Despite this predominant effect on the T_2 relaxation time, the properties of these agents on the T_1 relaxation time can also be exploited when appropriate imaging sequences are chosen [22,23]. The efficiency of a contrast agent or its relaxivity depends on its ability to accelerate the proton relaxation rate, which is defined as the increase of the relaxation rate of the protons of the solvent (water) induced by 1 mmol.L^{-1} of the active ion as described in Equation 2.

$$Ri(obs) = \frac{1}{Ti(obs)} = \frac{1}{Ti(dia)} + riC;\ i = 1\ or\ 2 \quad (2)$$

In this equation, $R_{i(obs)}$ and $1/T_{i(obs)}$ are the global relaxation rates in an aqueous system, $T_{i(dia)}$ is the relaxation time of the system before addition of the contrast agent, C is the concentration of the paramagnetic center expressed in mmol. L^{-1}, and r_i is the relaxivity (s^{-1}.mmol^{-1}.L). The effectiveness of a T_1 or T_2 contrast agent is defined by the r_2/r_1 ratio: the higher the ratio r_2/r_1, the more efficient the T_2 agent and the better the contrast. The magnetic relaxation characteristics can be measured by studying the nuclear magnetic resonance dispersion (NMRD) profile, which finally yields information about the mean crystal size, the specific magnetization,

and the Néel relaxation time [24]. The dipolar interactions between the superparamagnetic cores and surrounding solvent protons result in an increase in both longitudinal (spin-lattice) and transverse (spin-spin) relaxation rates and thus to an upgrade in the relaxivity; that is to say the effectiveness of the contrast agent. As examples, the r_1 values of commercial Resovist and Endorem are 25 $mM^{-1}.s^{-1}$ and 40 $mM^{-1}.s^{-1}$, respectively, at 0.47 T while their r_2 values was found to be 164 $mM^{-1}.s^{-1}$ and 160 $mM^{-1}.s^{-1}$ at the same magnetic field strength. Thus, the r_2/r_1 ratios of Resovist and Endorem are 6.2 and 4, respectively [25]. Interesting properties have also been obtained with non-commercial SPION [26,27].

Magnetic vehicles are very attractive for the delivery of therapeutic agents since they can be targeted to specific locations in the body through the application of a magnetic field gradient [28]. An estimate of the magnetic force exerted onto magnetic nanoparticles by a magnet can be calculated as:

$$\vec{F}_m = N_p \vec{m}_{eff} \nabla \vec{B} \quad (3)$$

where N_p is the number of magnetic nanoparticles, m_{eff} is the effective magnetic moment and $\tilde{N}B$ is the magnetic field gradient. Magnetic localization of a therapeutic agent allows it to be concentrated at the target site, thereby reducing or eliminating the systemic drug side effects. In magnetic targeting, carriers loaded with drugs and SPION are administered intravenously or intra-arterially. When an external high-gradient magnetic field is applied to the target site (ex: solid tumor), the magnetic moments of superparamagnetic particles are aligned with the field and the particles undergo a magnetophoretic driving force proportional to the field gradient which moves them toward the stronger field: in this way, the drug/SPION composites can be accumulated locally [29-31]. In most cases, the magnetic field gradient is generated by a strong permanent magnet, fixed outside the body over the target site. When the magnetic forces exceed the linear blood flow rates in arteries (10 cm/sec) or capillaries (0.05 cm/sec), the magnetic particles are retained at the target site by the external magnetic field. Once the carrier is concentrated at the targeted location, the drug can be released either by passive diffusion or by physiological triggers such as pH, osmolality, temperature, or enzymatic activity, or may be internalized, as intact SPION, by cells of the target tissue or tumor cells. The intravenous injection of magnetic nanocarriers needs to be balanced against a potentially higher reticuloendothelial system clearance and requires magnetic fields of sufficient energy [32,33]. The clinical success of magnetic drug targeting depends on strong magnets being able to produce high magnetic field gradients at the target sites and the method of their application.

Magnetic hyperthermia can also be the basis of a drug-free approach to the treatment of cancer by localized heating of cancer cells from the interior. When submitted to an alternating high-frequency magnetic field, magnetic fluids are able to release heat as a consequence of Neel and Brownian relaxation losses in single-domain particles [30,34,35]. Moderate raising the intracellular temperature to 41–47°C results in cancer cell apoptosis, whereas normal cells can tolerate this temperature [36,37]. Microenvironmental factors such as pH, oxygenation and blood perfusion can explain this tumor sensitivity [38]. The heating ability of a magnetic fluid is defined by the specific absorption rate (SAR), also called specific loss power (SLP), and is measured in Watts per g of magnetic material. It depends on the nature, the size and the structure of the particle [39]. Interesting and promising results have been obtained *in vivo* with this technique; for example, against osteosarcoma [40] and breast cancer [41].

A wide range of surface chemistry has been applied to SPION to design coatings that confer multiple functionalities onto each grain. These include modifications that permit the particles to avoid physiological barriers such as reticuloendothelial system, optimize circulation times, and maximize targeting and uptake by the desired cells, promote intracellular trafficking or enable controlled drug release. These strategies of direct modification of the iron nanoparticles are not discussed in this review but readers will find more information in dedicated review articles [42,43,44,45]. In this review, we consider lipid-based nanoassemblies containing SPION. These lipid nanoassemblies are classified into polar or non-polar lipid-based systems depending on the properties of the lipid material, mainly its interaction with bulk water and its behavior at the air-water interface [46]. According to this classification, some carriers are monophasic lipophilic nanodispersions and others are more complex constructs containing both lipidic and aqueous domains (Figure 1). Tables 1 and 2 summarize the properties of the different systems while Table 3 focuses on the *in vivo* applications of these SPION-loaded lipid-based nanoassemblies.

3. Magnetic-fluid-loaded lipid-based nanoscale systems

3.1. Systems based on polar lipids

3.1.1. Synthetic vesicles: liposomes

First described in the 1960s by Bangham [47], liposomes are core-shell structures defined as closed vesicles delimited by one or more concentric hydrated lipid bilayers that entrap a part of the aqueous phase in which they have been formed. Usually, the main component of liposomes is phospholipids. The drug delivery potential of these structures lies in their ability to incorporate hydrophobic or amphiphilic compounds in their bilayer shell and to encapsulate hydrophilic substances in their inner aqueous core. The latter property has been successfully exploited to load liposomes with a hydrophilic magnetic fluid that can be stabilized either through electrostatic repulsion of the iron oxide nanocrystals ensured by surface-binding of charged molecules, typically trisodium citrate, or through steric repulsion obtained by surface-coating with hydrophilic polymers such as chitosan, poly(ethylene glycol) (PEG), dextran, poly(vinyl alcohol) (PVA), poly(vinyl pyrrolidone) (PVP), and alginate [48,49,50,51,52,53]. Magnetic-fluid-loaded liposomes (MFL), also referred to as magnetoliposomes, have often been prepared by lipid film hydration with the aqueous suspension of superparamagnetic grains to be encapsulated, followed by sequential extrusion that provides calibrated unilamellar vesicles of submicronic size. The advantage of this procedure is that it preserves the individuality of

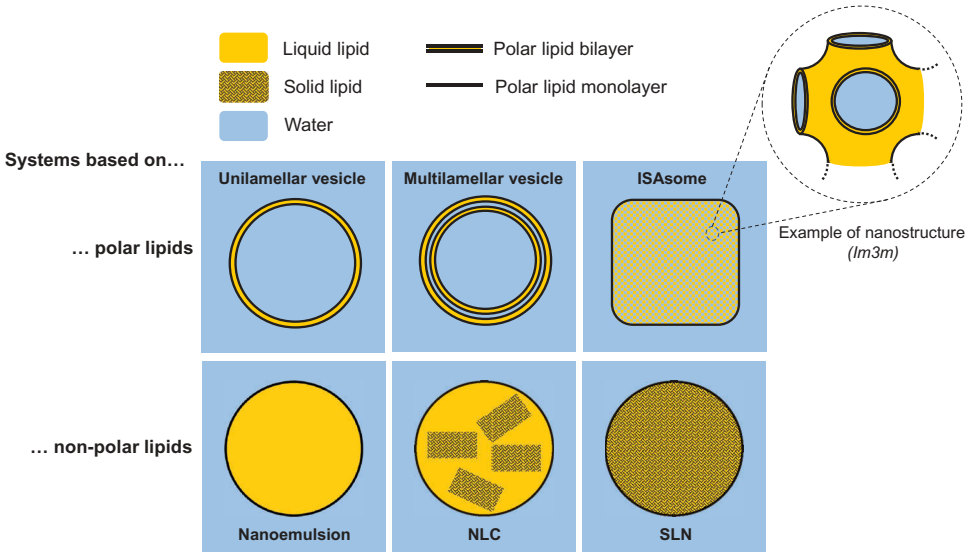

Figure 1. Schematic description of the classification used to organize the lipid-based nanosystems discussed in this review.

the iron oxide nanocrystals constituting the magnetic fluid and thereby their initial superparamagnetic behavior. A final, necessary, preparation step is liposome purification by removal of non-encapsulated material. While many original articles and several reviews [7,54,55,56,57] have been devoted to liposomes incorporating SPION, the following description focuses on systems in which drugs are co-encapsulated. They are classified according to the main role of the SPION.

3.1.1.1. Magnetic guidance. Martina et al. succeeded in producing MFL composed of egg-yolk L-α-phosphatidylcholine (EPC) with 1.2-diacyl-SN-glycero-3-phosphoethanolamine-*N*-[methoxy (poly (ethylene glycol))-2000] (DSPE-PEG_{2000}) as a steric stabilizer, encapsulating a concentrated suspension of maghemite nanoparticles obtained by coprecipitation of Fe^{2+}/Fe^{3+} salts and electrostatically stabilized with trisodium citrate [58]. Sequential extrusion followed by size exclusion chromatography to remove non-encapsulated material led to liposomes with a mean hydrodynamic diameter of 200 ± 50 nm and an iron loading of 0.53 ± 0.05 mol of Fe(III) per mole of total lipid (Figure 2(a)). The associate relaxivities were 18.6 ± 0.5 $mM^{-1}.s^{-1}$ and 116.0 ± 5.8 $mM^{-1}.s^{-1}$ at 0.47 T for r_1 and r_2, respectively, and the r_2/r_1 ratio is 6.2 whereas the relaxivities of the ferrofluid were 36,0 ± 1,0 $mM^{-1}.s^{-1}$ and 108.0 ± 5.4 $mM^{-1}.s^{-1}$ for r_1 and r_2, respectively, and the r_2/r_1 ratio is 3 under the same conditions [58]. The pharmacokinetic profile of these liposomes (200 µL of 200 nm-MFL, 20 mM total lipids, 34 mM Fe(III), 14 µg iron per g of mouse) indicated a biphasic elimination of the MFL from blood that consisted in a rapid elimination stage of MFL within the first two hours followed by a much slower elimination stage. The tissue distribution of SPION entrapped in MFL demonstrated preferential and progressive accumulation within liver and spleen [59]. As assessed by *in vivo* 7-T MRI and *ex vivo* electron spin resonance, 4 h exposure to a magnetic field gradient (155-T/m) efficiently concentrates MFL into human U87 glioblastoma implanted in the striatum of mice while avoiding healthy brain tissues [60]. When a lipophilic anti-estrogen (RU 58,668) was loaded into their bilayer by dissolving API and phospholipid during the film preparation, the liposomes gave promising results for the treatment of hormone-dependent breast cancer. Experiments on mice bearing MCF-7 xenografts have clearly shown that the accumulation of RU loaded-MFL at the tumor site is increased in the presence of magnetic field gradient and tumor growth can be significantly reduced compared with non-targeted tumors. The field-responsive behavior of magnetoliposome particles was demonstrated: the complete magnetic attraction of core/shell particles toward a 400 mT permanent magnet occurred in less than 2 min. Such magnetic responsiveness would provide a useful nanotool in accumulating an adequate dose of 5-FU into the tumor mass [61].

Fixed-dose combination products that consider the coadministration within a single vehicle of two or more drugs with synergistic activities have been attracting growing interest in the field of drug delivery. A first step toward combined chemotherapy was undertaken by Ye et al. in 2016 by developing gemcitabine and oxaliplatin-containing magnetoliposomes for breast cancer treatment [62]. In the optimal formulation, the lipid molar ratio was PC/cholesterol/dimyristoyl phosphatidyl glycerol 6:4:1. The mean hydrodynamic diameters of gemcitabine-containing magnetoliposomes (GML) and oxaliplatin-containing magnetoliposomes (OML) were 228 and 169 nm, the PdI of GML and OML were close to 0.133 and 0.060, and their drug-encapsulation efficiencies were 73% and 78%, respectively, after separation by size exclusion chromatography and magnetic sorting. Final concentrations higher than 1.5 and 0.25 mg/mL were obtained for gemcitabine and oxaliplatin, respectively. After IV administration, animal studies indicated that plasma gemcitabine and oxaliplatin levels were much higher with liposomal formulations compared with free API. Furthermore, under the guidance of an external magnetic field, drug-loaded magnetoliposomes accumulated in brain. Finally, magnetoliposomes significantly reduced the tumor size in BALB/c nude mice bearing MCF-7 cancer cells.

Table 1. Main characteristics of the systems based on lyotropic lipids

				SPION			Drug			
System type	Preparation process	Lipid composition	Mean diameter (nm)	Stabilizer	Concentration*	Encapsulation Efficiency	Name	Concentration*	Encapsulation efficiency	Ref
Liposomes	Ultrasonication	(1)	164	PEG	*200 mg/mL*	nd	Nimodipine	*>100 µg/mL*	95%	[55]
Liposomes	Film hydration + extrusion	DPPC Cholesterol	142–145	Citrate	Molar ratio (theoretical): 8 mol% vs. lipid	36%	Gemcitabine	Molar ratio (theoretical): 6 mol% vs. lipid	54%	[66]
Liposomes	Film hydration + extrusion	EPC-DSPE-PEG_{2000}	200	Citrate	0.53 ± 0.05 mol of Fe (III)/mol of total lipid	nd	RU 58,668	3.5 mol%	nd	[56,57,58,59]
Liposomes	Film hydration + extrusion	TMAG DLPC DOPE	100	nd	187 mg/ml	nd	Docetaxel	56.8 µg/ml	nd	[62,63]
Liposomes	Film hydration + extrusion	L-α-phosphatidylcholine cholesterol, stearylamine	150–200	Citrate	nd	nd	Cucurbit[7] uril zinc phthalocyanine complex	nd	nd	[64]
Liposomes	Reverse phase evaporation	DPPC DSPC DSPE-PEG_{2000}	150	Citrate	6 fg/liposome	nd	m-THPC	[m-THPC](µM)/[Fe](M) = 120 ± 15	nd	[65]
Liposomes	Film hydration + extrusion	PC	65	nd	nd	nd	5-fluorouracil	10^{-4} M	95%	[68]
Liposomes	Reverse phase evaporation + ultrasonication	Cholesterol DOPC- DPTAP- NBD-DPPE- PEG_{750}-DMPE- Fol-PEG_{2000}-DSPE	174	Oleic acid and hydrolyzed poly (maleic anhydride-alt-1-octadecane)	1 µM	89%	Doxorubicin	2 µM	nd	[69,70]
Liposomes	Reverse phase evaporation + ultrasonication	PC Cholesterol DMPG	228	nd	nd	68%	Gemcitabine Oxaliplatin	nd	73% 78%	[60]
Liposomes	Film hydration + ultrasonication	DPPC DOPG	227	Citrate	Mass ratio (theoretical): 25 wt% vs. lipid	83%	Paclitaxel	nd	75%	[67]
Microvesicles	Centrifugation Magnetic sorting	Natural membrane	670	Citrate	nd	nd	Foscan Doxorubicin t-PA TPCS2a	0.5 µM	nd	[77]
Exosomes	Conjugation	Natural membrane	40–110	Carboxyl-group	0.4 µg iron/µg exosome	nd	Doxorubicin	nd	10%	[78]
Cubosomes	Film hydration + sonication	Monoolein	230	Oleic acid	nd	nd	Rhodamine 110 Octadecyl rhodamine B	nd	17%	[86]

(1) Composition described in the supporting information which were not easily accessible. Data in italic have been calculated/estimated from the data available in the corresponding publications.

Table 2. Main characteristics of the systems based on non-polar lipids..

System type	Preparation process	Lipid composition	Mean diameter (nm)	Stabilizer	Concentration*	Encapsulation Efficiency	Name	Concentration*	Encapsulation efficiency	Ref
Nanoemulsions	Solvent removing + sonication	DSPC PEG–DSPE soybean oil Cy5.5 PEG–DSPE	50	Oleic acid	*375 µg/mL*	100%	Prednisolone acetate valerate	*0.13 mg/mL*	68%	[110,111,112]
Solid lipid nanoparticles	oil-in-water emulsion + sonication	Cetyl palmitate	248	Unknown polymer (commercial SPION)	3 wt%	*>80%*	Sorafenib	$6.35.10^{-6}$ M	90%	[121]
Solid lipid nanoparticles	Film scattering + sonication	GMS HSPC F-68	224	Oleic acid	2.16 mg/mL	nd	Cisplatin	nd	69%	[122]
Solid lipid nanoparticles	Ultrasonic dispersion	Stearic acid	127	Oleic acid	nd	nd	Ibuprofen	nd	80%	[124]
Solid lipid nanoparticles	Solvent diffusion	Monostearin	228	Oleic acid	nd	19–83%	Doxorubicin	3%	65%	[125]
Solid lipid nanoparticles	Oil-in-water emulsion + homogenization	Trilaurin	100–180	Octadecyltrimethoxy-silane	20 mg/mL	40–65%	Tetracaine	$1.3.10^{-3}$ M	nd	[126]
Solid lipid nanoparticles	High shear homogenization	Cetyl palmitate Stearic acid Tween 60	206	Oleic acid	1 wt%	nd	Methotrexate	1 wt%	98%	[128]
Solid lipid nanoparticles	Solvent diffusion	Nucleolipids DOPC	100–150	Nucleolipids	*100 µg/mL*	nd	α-tocopherol Prostacyclin	*0.05 mg/mL*	10%	[123]

Data in italic have been calculated/estimated from the data available in the corresponding publications.

Table 3. Summary of the *in vivo* biological evaluations made with the systems described in this review.

			In vivo evaluation						
System type	Drug	Objectives	Model	Administration route	SPION dose	Drug dose	Magnetic field parameters	Main results	Ref
Liposomes	Nimodipine	Magnetic guidance Imaging Early diagnosis Chemotherapy	Parkinson disease rat model (6-OHDA injection)	IP	nd	1 mg/kg/day	Magnet D10×5 mm, N35 Imaged at a 3T MRI	2.5× increase of drug concentration compared to drug solution Neuroprotective effect of drug loaded liposomes	[55]
Liposomes	RU 58,668	Imaging Magnetic guidance Chemotherapy	Human U87 glioblastoma	IV	12.8 µmol/g	0.15 µmol	Imaged at a 7T MRI	Magnetic accumulation of RU-MFLs RU 58,668 anti-proliferative activity	[56,57,58,59]
Liposomes	Docetaxel	Chemotherapy Hyperthermia	Human MKN45 gastric cancer cells in Balb-c/nu/nu mice	IV	nd	7.5–15 mg/kg	a 6.36-kA/m magnetic field alternating at 478 kHz with an output power of 1 kW	Reduction of tumor volume Increase in survival rate	[62,63]
Liposomes	Gemcitabine Oxaliplatin	Chemotherapy	MCF-7 cell in BALB/c nude mice	IV	nd	9–35 µg/g 1.25–5 mg/kg	5000 G	Minimization of tumor size Inhibition of MCF-7cell growth	[60]
Liposome	Foscan	Imaging Hyperthermia Phototherapy	Carcinoma A431 cells into NMRI nude mice	Intratumoral	*90 mg/kg*	*0.16 mg/kg*	30 mT at 111 kHz for 30 min Imaged at 4.7 T	Complete tumor regression with the dual therapy	[65]
Exosomes	Doxorubicin	Chemotherapy	Kunming mice bearing a subcutaneous H22 cancer	IV	nd	5 mg/kg	Magnet 1T	Enhancement of cancer targeting under external magnetic field Suppression of tumor growth	[77]
Nanoemulsion functionalized with RGD peptide	Prednisolone valerate acetate	Imaging Chemotherapy	Colon cancer model (LS174T) in Swiss nude mice	IV (tail vein)	30 mg/kg	10 mg/kg	Imaged at a 3T whole body MR scanner	Significant accumulation of the nanoemulsion in the tumors. Potent inhibitory effect on tumor growth in all animals treated with drug loaded nanoemulsion.	[110,111,112]
Magnetic Solid Lipid Nanoparticles	Cisplatin	Therapeutic	Human cervical carcinoma SiHa cells into female nude mice (B AIB/C)	IV (tail vein)	nd	0.6 mg/kg	Cylindrical rubidium iron boron rare earth magnet (4500 G)	High drug concentrations	[122]

Data in italic have been calculated/estimated from the data available in the corresponding publications.

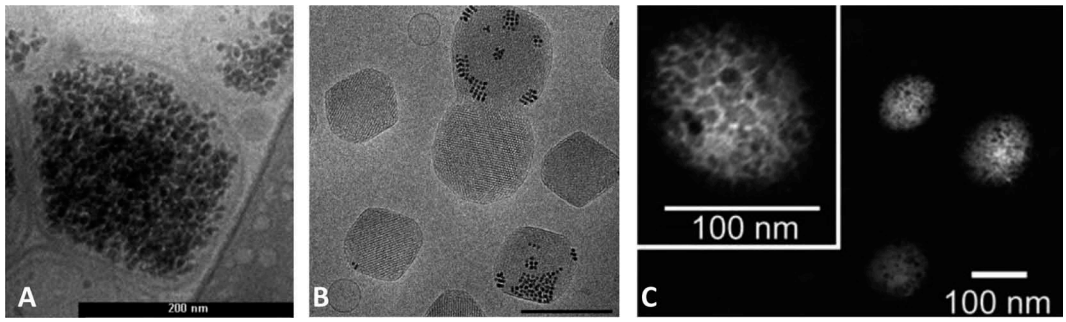

Figure 2. TEM or cryo-TEM micrographs of the main superparamagnetic lipid-based nanosystems discussed in this review: a – liposomes ([58], scale bar: 200 nm); b – cubosomes ([87], scale bar: 200 nm); c – nanoemulsions ([112], scale bar: 100 nm) [126]. Dense grains correspond to SPION. Figures reproduced with permission.

3.1.1.2. Hyperthermia. Pioneer work coupling hyperthermia with drug release, in this case 5-fluorouracil (5-FU), was carried out twenty years ago in Horikoshi's group [63]. More recently, Yoshida et al. studied the effectiveness of chemo-hyperthermia with docetaxel-bearing cationic magnetoliposomes (DML) and an applied alternating current magnetic field. The DML had an average hydrodynamic diameter about 100 nm and the mean magnetite concentration was 187 ± 22 mg/mL. In the mice that were injected (IV) with DML at a docetaxel concentration of 57 µg/mL and exposed to an alternative current magnetic field of 1 kW, tumor size was significantly decreased after treatment. The tumor disappeared in 3 mice in the DML group exposed to the magnetic field, 2 mice survived more than 6 months after treatment, whereas all mice in the other groups died after 15 weeks. Histological investigation demonstrated that DML diffuse homogeneously and DML-mediated hyperthermia damaged tumor cells [64]. Moreover, docetaxel and tumor necrosis factor-α concentration, the cell cycle, and cell death rates in the tumor were examined. Three days after injection, the docetaxel concentrations were significantly higher in the DML-treated groups compared with injection of free drug. The rate of tumor cell death increased in the DML-treated group, with or without hyperthermia, and the tumor necrosis factor-α concentration in the tumor treated with DML with heating remained at a high level on the 7th day after treatment, while it decreased after one day in other groups [65].

Other therapeutic modalities of magnetoliposome have been tested, including the combination of hyperthermia and a photodynamic effect on melanoma by preparing stearylamine-containing magnetoliposome loaded with cucurbit-7-uril zinc phthalocyanine complex (CB:ZnPc) and citrate-coated SPION. The authors made a lipid film of soya phosphatidylcholine, cholesterol, stearylamine and the CB:ZnPc and after hydration with phosphate buffer solution (10 mM, pH 7.4) and extrusion (1–0.1 µm), a suspension of calibrated liposomes was obtained (150–200 nm). Hyperthermia was investigated in combination with photodynamic therapy on melanoma cells (B16-F10) and the *in vitro* results showed that magneto-hyperthermia can act synergistically with the photodynamic effect [66]. For example, B16-F10 cells treated with the highest light dose (2.0 J cm^{-2}) and subsequent AC magnetic field activation (1 MHz and 40 Oe amplitude, during 3 min) had their viability reduced to about 13%. The same combined therapy was investigated with DPPC/DSPC/DSPE-PEG2000 liposomes loaded with Foscan, a photosensitizer, and citrated SPION [67]. The comparison between *in vitro* (Human adenocarcinoma SKOV-3 cells) and *in vivo* (epidermoid carcinoma A431 cells in NMRI nude mice) results is very interesting here since photodynamic therapy was more effective *in vitro* and magnetic therapy *in vivo*. Nevertheless, the combination of the two therapies yielded the best results both *in vitro* and *in vivo*.

Interestingly, the release of the drug can be controlled by the liposomal carrier and/or by the hyperthermia effect. Ferreira et al. reported the preparation and characterization of thermosensitive magnetoliposomes containing gemcitabine for combined hyperthermia and chemotherapy. These unilamellar liposomes had a hydrodynamic diameter of 145 nm, a polydispersity index (PdI) of 0.10 and a zeta potential of −9 mV. The encapsulation efficiencies of the gemcitabine and SPION in magnetoliposomes were 54% and 36%, respectively. For effective hyperthermia therapy, the temperature of tumor tissue must reach 42–45°C. Here, when the samples were exposed to an alternating magnetic field (AMF) of 356 kHz for 5 min, the temperature ranged from 32°C to approximately 56°C which is appropriate for effective hyperthermia treatments. AMF-triggered local heating induces fluidification of the DPPC/cholesterol bilayer which becomes more permeable. As a result, a 70% drug release was observed after 5 min of exposure compared with around 10% after 72 h at 37°C [68]. Kulshrestha et al. obtained the same type of results with paclitaxel-loaded DPPC/DOPG-based magnetoliposomes [69]. In this study, only 1.2% of the drug was released after 30 min at 37°C while under AMF (10 kA/m; 423 kHz), the temperature was raised to 43°C and the release to 55.6%.

A more controlled release was obtained with multilamellar magnetoliposomes that had a mean hydrodynamic size of 65 ± 20 nm, and were loaded with 5-FU, designed for use against colon cancer. On exposure to a high frequency magnetic field gradient, the oscillation of the magnetic moment of the magnetoliposomes produced a heating effect, reaching the minimum hyperthermia temperature (41°C) in 22 min and a maximum temperature (45°C) after 27 min. The release of 5-FU entrapped within the magnetoliposomes showed first-order kinetics, since the release rate decreased with time. When the release medium was coupled to a high-frequency alternating electromagnetic field (250 kHz, 4 kA/m), 5-FU

release was significantly accelerated but remained prolonged [70].

Chen et al. developed PEG-stabilized magnetoliposomes containing both SPION in their bilayer shell and the anticancer drug doxorubicin as a stimuli-responsive drug delivery system for low-dose chemotherapy [71]. This system referred to as dMLS was prepared by a reverse-phase evaporation method from a chloroform solution of the component lipids (DPPC/DSPE-PEG_{750} at 95:5 mol%) and commercial SPION stabilized with oleic acid (OA-SPION) mixed with an aqueous solution doxorubicin in phosphate buffer PBS. Liposome calibration was carried out by extrusion and the final dMLs were characterized by a mean hydrodynamic diameter of ~120 nm. Low-dose chemotherapy of Huh-7 cells was achieved by radio frequency-triggered release of doxorubicin from dMLs based on increased fluidity of the phospholipid bilayer when the temperature was raised. Uptake of the dML by the cells was governed by diffusion within the culture media, consistent with a non-targeted delivery vehicle [71]. The role of SPION here is to allow local heating by Neel and Brownian relaxation losses.

To improve the selectivity of treatment, it is possible to graft specific ligands for biochemical targeting onto the surface of drug-loaded magnetoliposomes. Folate-targeted cationic magnetoliposomes (FTMLs) composed of 1,2-dioleoyl-sn-glycero-3-phosphocholine (DOPC), 1,2-dipalmitoyl-3-trimethylammonium propane (DPTAP), 1,2-dipalmitoyl-sn-glycero-3-phosphoethanolamine-N-(7-nitro-2–1,3-benzoxadiazol-4-yl) (NBD-DPPE), 1,2-dimyristoyl-sn-glycero-3-phosphoethanolamine-N-[methoxy(polyethylene glycol)-750] (PEG750-DMPE), and 1,2-distearoyl-sn-glycero-3-phosphoethanolamine-N-[folate (polyethylene glycol)-2000] (Fol-DSPE-PEG_{2000}) with co-encapsulated doxorubicin have been prepared [72]. FTMLs were prepared at 10 mM total lipid by thin film hydration followed by extrusion and centrifugation was used to remove non-encapsulated SPION. The final magnetoliposomes were characterized by an average static diameter of 174 ± 53 nm estimated by cryoTEM and a SPION encapsulation efficiency of 89% determined by inductively coupled plasma mass spectrometry. Cell uptake experiments were carried out on HeLa (cervical cancer cells) and ZR-75 (human breast carcinoma) cell lines to assess targeting efficiency. The internalization of FTMLs or MFL (without folate receptor targeting lipid) by HeLa cells showed no difference up to 120 min but was greater with FTMLs at 180 min. In contrast, no FTML or MFL uptake was observed in ZR-75–1 cells. This result is consistent with FOLR1 expression results, where HeLa cells showed 42.5-fold greater expression than ZR-75–1 [72]. With radio frequency heating similar to that used for tumor ablation, a threefold increase in doxorubicin release was observed.

3.1.2. Natural vesicles: microvesicles and exosomes

Microvesicles and exosomes are vesicles produced endogenously by mammalian cells [73]. Microvesicles have a size range of 100–1000 nm while exosomes are smaller, between 30 and 100 nm. These extracellular vesicles carry lipids, proteins, receptors, and effector molecules and participate in distant intercellular communication. In terms of their mechanisms of formation, briefly, microvesicles originate from the budding of the plasma membrane while exosomes are derived from endosomes formed from plasma membrane [74]. Interestingly, after isolation by differential centrifugation or magnetic sorting with magnetic antibodies, these natural vesicles show excellent *in vivo* stability, are less cytotoxic than synthetic vesicles [75] and can be loaded with SPION [76,77,78]. Silva et al. produced microvesicles loaded with SPION and four different drugs, a clinical photosensitizer drug (Foscan), disulfonated tetraphenylchlorin (TPCS2a), doxorubicin, and tissue-plasminogen activator (t-PA), to rank them from the least to the most hydrophilic [79]. Microvesicles with a size of around 670 nm and PdI ~0.3 were obtained after 2 h incubation of THP-1 macrophages with SPION and the drug of interest, serum depletion to induce a proapoptotic stimulus and cell stress, then isolation by magnetic sorting after centrifugation to eliminate apoptotic bodies and dead cells. Magnetophoresis experiments confirmed the co-encapsulation of SPION and fluorescent drugs. Finally, spatial targeting using a magnet as well as a therapeutic effect has been demonstrated *in vitro* on SKOV-3 human ovarian cancer cells and PC-3 human prostate cancer cells with the system incorporating Foscan. More precisely, the distribution of fluorescent microvesicles and the necrosis domains after generation of a magnetic field gradient along the culture surface and irradiation of the entire plate at 650 nm confirmed that the two agents remained co-encapsulated and the endocytosis of microvesicles. Qi et al. recently developed a dual-functional exosome-based superparamagnetic nanoparticle cluster for tumor-targeting drug delivery. Briefly, fresh serum was collected from healthy Kunming mice and predialyzed against PBS. The conjugation of holo-transferrins to carboxyl-group-functionalized Fe_3O_4 nanoparticles leads to the formation of iron-loaded transferrins (M-Tfs). Incubation of M-Tfs with the predialyzed serum allowed multiple M-Tfs to bind to each reticulocyte-derived exosome through a Tf–Tf receptor interaction to form reticulocytes-exosome-based superparamagnetic nanoparticle cluster (SMNC-EXOs) with a concentration of 0.40–0.45 μg iron/μg exosome. These clusters were then purified by magnetic separation and redispersed into PBS. SMNC-EXOs were incubated in the presence of doxorubicin in order to form drug-loaded SMNC-EXOs (D-SMNC-EXOs) with hydrodynamic diameters in the 40–110 nm range. Quantitative analysis by UV-visible absorption indicated a doxorubicin entrapment efficiency of 10%. After IV injection into homologous mice bearing subcutaneous hepatoma 22 cancer cells, D-SMNC-EXOs accumulated in the tumor region and released doxorubicin to suppress tumor growth when an external magnetic field was applied [80]. Very recently, Piffoux et al. compared different methods of producing exosomes containing SPION and Foscan, notably by spontaneous release in complete medium, starvation in serum-free medium, and microfluidic-based mechanical stress [81]. The impact of the production and purification protocols on SPION and photosensitizer loading, yield and purity was investigated and results suggested that starvation combined with ultracentrifugation gave the best trade-off.

3.1.3. Internally self-assembled particles

Bicontinuous cubic lipid phases consist of a single lipid bilayer membrane that adapts an infinite periodic minimal surface dividing the space into two non-intersecting networks of water

channels. This particular liquid crystalline state forms spontaneously under appropriate conditions upon mixing some lyotropic lipids with various polar head groups with water, the lipids most often used being monoglycerides [82, 83]. In excess water, application of high-energy dispersion, i.e. sonication or homogenization, can lead to nanoscale particles or ISAsomes (internally self-assembled 'somes'), typically ranging from 10 to 500 nm in size and of well-established biocompatibility [84,85]. Depending on their internal organization, which can be mainly bicontinuous cubic or reverse hexagonal phases, two types of particle have been described: cubosomes and hexosomes. These can be stabilized using surfactants, e.g. poloxamer 407, or hydrophilic polymers, e.g. polyvinyl alcohol, in proportions generally not exceeding from 2.5% to 10% w/w with respect to the total weight of the dispersion. Due to their small pore size (5–10 nm) and their ability to solubilize hydrophobic, hydrophilic, and amphiphilic molecules, cubosomes have many potential applications in the field of oral, topical and intravenous drug delivery systems [86].

Acharya et al. described the preparation of hybrid superparamagnetic mesophase nanoparticles (HMNs). In this system, OA-SPION were dispersed in the cubic phase forming the glycolipidic (phytantriol) matrix of the nanoparticles. These cubosomes have a hydrodynamic diameter of 180 nm and the SPION concentration used (0.3 wt% Fe in phytantriol) did not compromise the internal structure of the bicontinuous cubic phase. Transverse relaxivity (r_2) measurements show that enhancement of the transverse relaxivity r_2 of the magnetic cubosomes was proportional to the loading of OA-SPION in the mesophase nanoparticles although the load seemed to be heterogeneously distributed within the bicontinuous lipid dispersion (Figure 2(b)) [87].

More recently, Montis et al. developed a new nanostructured drug delivery by including OA-SPION in the bilayer membrane of bicontinuous cubic lipid nanoparticles of glyceryl monooleate (monoolein). The first results showed that these magnetocubosomes were able to host both model hydrophilic and hydrophobic molecules, rhodamine 110 and octadecyl rhodamine B, respectively, in separate compartments, and to release the payload in a space and time-controlled manner, upon application of a low-frequency alternative magnetic field of 6 kHz. Magnetic-field-induced structural destabilization of the bilayer of the cubosomes with the formation of pores allowed the escape of drugs from the aqueous channels, acting as a release trigger [88].

Hong et al. prepared iron oxide nanoparticles within a monoolein cubic phase. The cubic phase was obtained by hydrating molten monoolein with an aqueous Fe^{2+}/Fe^{3+} salt solution that was allowed to co-precipitate with an alkali solution into SPION inside the aqueous channels delimited by the monoolein bilayer. Micronizing these cubic phases finally led to the formation of superparamagnetic cubosomes, responsive to a magnet, and the magnetic interaction degree, measured by the percent of decrease in monoolein concentration after magnetic fields were applied to cubosome suspensions, was proportional to the amount of SPION formed within the cubic phases [89]. These authors also tried to form similar particles from a mixture of monoolein and oleic acid (OA), the latter being included in the cubosomes in order to electrostatically adsorb Fe^{2+}/Fe^{3+} at the lipid – water interface. To control and trigger the drug release, a thermosensitive polymer, poly(N-isopropylacrylamide), was dissolved in the water phase in order to increase its viscosity. Under an alternating magnetic field, magnetite in the cubosome will produce heat and increase the temperature of the medium. Consequently, poly(N-isopropylacrylamide) immobilized in the water channel undergoes a phase transition, reducing the viscosity and controlling the drug release from the cubosomes [90].

3.2. Systems based on non-polar lipids

3.2.1. Nanoemulsions

Nanoemulsions, defined as liquid-liquid biphasic dispersions at the nanometer scale, have attracted growing interest as colloidal drug carriers, notably for intravenous administration, from parenteral nutrition to drug transportation [91,92,93], or for oral administration of poorly water-soluble drugs since they have been shown to increase drug bioavailability through enhancement of intestinal absorption [94]. Furthermore, the specific advantages of nanoemulsions over other nanotechnologies used for drug delivery are their high loading capacity for lipophilic drugs, formulation stability, ease of manufacture, and their relatively low complexity [95]. Nanoemulsion-based systems for the prevention and treatment of cancer, inflammatory diseases and adjuvant delivery in immunotherapy have been investigated and marketed [96,97,98,99]. Nanoemulsions can be prepared by two major techniques, i.e. high-energy and low-energy emulsifications. High-energy emulsification methods include high-shear stirring, high-pressure homogenization and ultrasound generators. Low-energy emulsification methods are emulsification methods making use of the chemical energy stored in the components and are receiving increased attention. In these methods, nanoemulsions are obtained as a result of phase transitions produced during the emulsification process [100].

Pharmaceutically used and approved nanoemulsions are mostly composed of an oil phase dispersed in a continuous aqueous phase as droplets with submicronic size, preferentially with maximum radius below 200 nm [63]. As far as SPION-loaded nanoemulsions are concerned, the iron oxide nanoparticles were stabilized in the oil phase by coating them with hydrocarbon chains by binding oleic acid through its carboxylic head group (OA-SPION) [101,102,103], phosphoesters via their phosphonates head group [104,105,106,107] or silanes derivatives [108,109,110,111].

Jarzyna et al. developed a bimodalplatform by co-incorporating a near-infrared fluorescent lipid dye, Cy5.5-PEG-DSPE, and commercially available OA-SPION based on magnetite in nanoemulsion droplets. These were composed of a hydrophobic oil core made of soybean oil and stabilized by distearoyl phosphatidylcholine (DSPC) and DSPE-PEG_{2000}. Chloroform solution of each component were mixed together, dispersed dropwise in boiling water and then sonicated and concentrated in order to form calibrated droplets with mean hydrodynamic diameters of 30, 60, or 95 nm (Figure 2(c)), depending on the relative proportions of the different lipids. Inductively coupled plasma mass spectrometry (ICPMS)

analysis revealed almost 100% encapsulation efficacy of magnetite, that is, a similar SPION number to droplet volume ratio, leading to r_1 values of 2.5 ± 0.4 $mM^{-1}s^{-1}$, to 2.7 ± 0.3 $mM^{-1}s^{-1}$, to 2.9 ± 0.3 $mM^{-1}s^{-1}$ at 1.41 T for the 30, 60, and 95 nm emulsions, respectively and high r_2 values of 76 ± 1 $mM^{-1}s^{-1}$, 136 ± 9 $mM^{-1}s^{-1}$, or 184 ± 7 $mM^{-1}s^{-1}$ at the same field for nanoemulsions of 30, 60, or 95 nm in droplet diameter, respectively. The conjugation of a near-infrared fluorophore that allowed optical imaging demonstrated the accumulation of this nanocomposite in subcutaneous human tumors in nude mice, which was confirmed with MRI imaging *in vivo* [112].

To go further, the same team functionalized the nanoemulsion with $\alpha_v\beta_3$-specific RGD peptides to enable specific molecular MRI and optical imaging of tumor angiogenesis. The cyclic peptide RGD was conjugated to the nanoemulsion droplets coated with DSPE-PEG-maleimide units by the sulfhydryl-maleimide coupling method, resulting in a nanoemulsion (RGD-NE) with a mean droplet diameter of 90 ± 10 nm. MR images at 3T after IV injection of RGD-NE showed a lowering of signal intensity in the tumor periphery where angiogenesis activity is the highest. RGD-NE fluorescence was found co-localized with endothelial cell staining, as observed in tumor sections [113]. The latest advance for this system was to incorporate a hydrophobic drug, prednisolone valerate acetate (PAV), for theranostic applications. In this case, PAV was included in the lipophilic phase during the fabrication process, leading to nanoemulsions with droplet mean diameter of 53 nm. This system has proven its efficiency in tumor growth inhibition in mice after intravenous injection compared with drug-free nanoemulsions, SPION-loaded nanoemulsions and an ethanolic solution of PAV at a dose of 10 mg PAV/kg [114].

3.2.2. Solid lipid nanoparticles

Unlike nanoemulsions that are constituted by lipids in their liquid state only, solid lipid nanoparticles (SLN), and nanostructured lipid carriers (NLC) result from the dispersion in an aqueous phase of lipids which are totally (SLN) or partly (NLC) in their solid state. SLN are usually composed of non-polar lipids such as long-chain glycerides, waxes, or fatty acids [115,116,117,118,119,120,121] that are cystalline at room temperature while NLC are produced by mixing solid and liquid (oil) lipids at the same temperature [120]. Both systems result from the dispersion of the lipids into a liquid state, by melting or dissolution in a suitable solvent, followed by solidification of the droplets by cooling or solvent evaporation. The small size of the particles is obtained by use of high-energy dispersion (as for nanoemulsions) or solvent diffusion – evaporation phenomenon. The SPION are similar to those incorporated into nanoemulsions.

The first reported SLN system encapsulating magnetite was described in 1996 by Muller et al. It was composed of trilaurin and Poloxamer 188 as stabilizer and obtained by high-pressure homogenization [122]. Grillone et al. describe the development of Sorafenib-loaded magnetic SLN using cetyl palmitate as the lipid matrix. To obtain this system, the lipid, commercially available lipophilic SPION and Sorafenib were dissolved into solvents and added to a hydrophilic phase containing Tween 80 in water at 75°C. This oil-in-water emulsion was homogenized using sonication at elevated temperature to evaporate the solvents. The final dispersion was maintained at 4°C to allow the crystallization of the lipids and the formation of the SLN with an average hydrodynamic diameter of 248 ± 113 nm. A SPION loading of about 3 wt%, with respect to the lipids, could be estimated by thermogravimetric analysis whereas the encapsulation efficiency of Sorafenib was about 90%, assessed by UV–visible absorption. The resulting magnetic SLN did not significantly alter the viability of HepG2 cells and those loaded with Sorafenib were able to inhibit cancer cell proliferation through the cytotoxic action of drug, and to enhance/localize this effect in a desired area thanks to a magnetically driven accumulation of the drug with a 1.32 T permanent neodymium magnet. The quantitative determination of cell mortality, evaluated as percentage of cells positive for binding ethidium homodimer-1, was shown to be about 95% in the channel close to the magnet, and 5% in the control compartment [123].

Zhao et al. described the preparation and the characterization of cisplatin-loaded magnetic SLN by a film scattering ultrasonic technique. The results are very promising in terms of drug and OA-SPION loading and the *in vivo* response to an external magnetic field [124]. A magnet fixed in the upper left abdomen of Kunming mice allowed cisplatin accumulation in tissues adjacent to the magnetic field (kidney, liver), as well as reduced concentrations in tissues far from the magnet such as brain and heart, compared with distribution studies without an external magnetic field. However, the high encapsulation efficiency (69 ± 4%) of the drug, which is hydrophilic, by these hydrophobic particles should be investigated more carefully. Less classically, SLN could also be formed with nucleolipids in order to produce promising neutral or charged nanoparticles that have been loaded with SPION and α-tocopherol or Prostacyclin for image-guided therapy of atherosclerosis [125].

The release kinetics of drugs carried by magnetic SLN has been investigated. Two types of behavior have been observed depending on whether a prolonged release process or a triggered release was required. The first approach aimed at showing the stability of drug incorporation in the magnetic lipid particles while the second one focused on the possibility of controlling the drug release by submitting the co-encapsulated SPION to an alternative magnetic field. Pang et al. prepared by ultrasonic dispersion SLN composed of stearic acid and loaded with OA-SPION as well as with ibuprofen. The resulting ibuprofen-loaded magnetic SLN (IBMSLN) were characterized by an average hydrodynamic diameter of 127 ± 17 nm and drug encapsulation efficiency close to 80% (Figure 2(d)). Superconducting quantum interference device (SQUID) measurements indicated that IBMSLN exhibit superparamagnetic behavior with a blocking temperature of 86 K. The cumulative passive drug release from IBMSLN was 2%, 27%, and 78% after 1, 8, and 40 h, respectively, while the pure ibuprofen was totally dissolved in less than 8 h. The ibuprofen release results show that the drug release by diffusion can be controlled in the magnetic nanoparticles, which act as a matrix, and make this system a potentially useful tool for drug delivery [126]. Similar passively controlled release formulations have been described by Ying et al. with magnetic monostearin-based SLN carrying doxorubicin [127].

To obtain triggered release, Hsu et al. developed another SLN system in which γ-Fe_2O_3 nanoparticles were surface-grafted with octadecyltrimethoxysilane groups. These

lipophilic SPION were then dispersed and stirred in a melted lipid matrix composed of trilaurin and containing a lipophilic drug (tetracaine) before being emulsified in an aqueous solution of a surfactant (Poloxamer 188). Afterward, the lipid-in-water emulsion was refined using a high-pressure homogenizer to decrease the droplet size. Finally, the lipid-in-water emulsion was cooled to form magnetic SLN with average hydrodynamic diameters between 100 and 180 nm. When exposed to an alternative magnetic field of 60 kA/m at 25 kHz, magnetic SLN showed a significant increase in temperature of up to 8°C. At the same time, the dissipated heat melted the lipids surrounding the iron oxide grains resulting in an accelerated release of the encapsulated drug. The authors observed that after a heating period of 20 min, 35% of the initially encapsulated tetracaine was released from the lipid nanoparticles while without heating, the tetracaine release over a 30-day period at room temperature was found to be less than that stimulated by a 5-min exposure to magnetic heating [128].

Similarly to liposomes, biochemical targeting of SPION-loaded SLN has been investigated. Thus, Albuquerque et al. combined high shear homogenization and ultra-sonication to develop a new theranostic tool for early detection by MRI imaging and treatment of rheumatoid arthritis by intravenous administration of a formulation consisting of methotrexate (MTX)-loaded SLN incorporating OA-SPION using an organic solvent-free method. These SLN were functionalized with a monoclonal antibody directed against the macrophage-specific cell surface receptor, CD64, overexpressed in rheumatoid arthritis. Solid lipids (cetyl palmitate, stearic acid and Tween 60) were heated to 70°C and mixed with MTX, OA-SPION, and water. The resulting emulsion was immediately homogenized by sonication and cooled to produce the SLN. The SLN were then functionalized with the anti-CD64 antibody. Monodisperse nanoparticles with a hydrodynamic diameter of 206 ± 3 nm were yielded with a 98% MTX encapsulation rate. Transmission electron microscopy images indicated that the SPION were encapsulated within the lipid matrix. MTT assays on THP-1 macrophages indicated that the antibody-conjugated formulations did not cause any significant difference in viability compared with non-conjugated ones, except at the highest concentrations. These results showed that the conjugation of SLN with the anti-CD64 did not alter their biocompatibility and confirmed their potential for biomedical applications, notably in the field of rheumatoid arthritis [129].

4. Conclusion

All the lipid-based nanoscale assemblies described here were specifically designed to allow double incorporation of a superparamagnetic nanomaterial (SPION) and a drug. A priori, the expected benefits provided by the superparamagnetic behavior of SPION fall into three applications: (i) the possibility of monitoring or controlling the distribution of the nanocarrier in the body and thereby, theoretically, that of the drug by applying a suitable magnetic force, (ii) the triggering of drug release, or (iii) the implementation of a synergistic hyperthermia treatment to conventional chemotherapeutics, the two last applications being based on a heating effect produced by an up-and-down magnetization process under an alternating magnetic field. It appears that very few studies have focused on all the three pathways, i.e. on targeted theranostic tools, leaving a need for further work on this aspect.

5. Expert opinion: a focus on co-encapsulation

Different modes of organization of the final hybrid systems have been investigated, depending on the nature of the lipids and their related hydration behavior. The crucial steps in building the systems are, first, to tailor the surface-stabilization of the iron oxide nanocrystals to the type of inner reservoir into which they will be loaded; that is, hydrophilic or lipophilic and, secondly, to implement a reliable method of incorporation to optimize loading rates. It follows that it is also necessary to investigate the influence of SPION encapsulation on that of the drug and the ability to obtain a constant drug-to-SPION ratio within the same nano-object. In this respect, let us consider in depth some of the reported observations. The work on folate-coated liposomes by Bothun et al. clearly reveals an heterogeneous distribution of the encapsulated hydrophilic SPION among the magnetoliposomes obtained, some of which contained no SPION, others contained individual grains and still others were filled with SPION clusters [72]. This agrees with independent findings on magnetic-fluid-loaded liposomes (MFL) for which a given vesicle population entraps variable numbers of iron oxide particles [7]. This phenomenon means that the evaluated encapsulation efficiencies reflect an average of iron oxide loading and coexistance in each preparation of nano-objects with different responsiveness to magnetic fields. To reduce this heterogeneity, magnetic sorting has been performed to remove empty or low-loading-rate vesicles from MFL preparations [60]; however, this procedure has not been used routinely. Considering other compartmented nanosystems such as cubosomes, the SPION-containing areas are also non-uniformly distributed through the inner structure of these assemblies and SPION-free areas can be observed, leading to coexisting magnetic and non-magnetic objects as shown in Figure 3. In fact, the heterogeneity of SPION distribution observed in most of the compartmented nanoscale systems probably arises because the incorporation of the iron oxide nanocrystals usually involves a two-step protocol: (i) the introduction of SPION during the mixing of the constituting lipids, possibly before solubilization in an organic solvent, and the aqueous phase in which they will be allowed to self-organize, (ii) homogenization of the mixture and nanoscale fragmentation. Mainly as a result of the slow kinetics of both lipid hydration and solvent diffusivity coupled with the limited diffusion rate of colloidal iron oxide due to their size and the viscosity of the medium, the first step presents an intrinsic risk of non-uniform distribution, all the more so because the preparation is performed in bulk. Therefore, since the second step consists in dispersing the system into separate subunits, it necessarily generates a population of nano-objects containing different amounts of SPION. As well as being a simple reflection of the non-

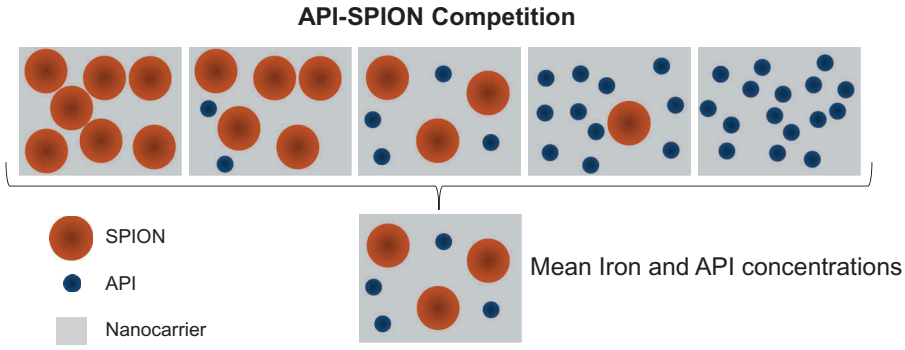

Figure 3. Schematic description of the competition between SPION and API for encapsulation in the nanocarrier.

homogenous distribution of SPION in the initial bulk mixture, it is also possible that, considering the dimension of the incorporated SPION, the probability of finding them in a given nano-object closely depends on the volume of the host compartment, the smaller this volume the lower the trapping probability. This is notably the case for liposome-based systems since extrusion or sonication or even high-pressure shear homogenization leads to small calibrated vesicle structures through successive breaks and closures of the lipid bilayer. As far as non-lamellar assemblies such as those issued from bicontinuous cubic phases are concerned, it is worth noting that these organizations are unclosed structures so that the increase in the cumulative interface with the surrounding continuous aqueous phase generated by the fragmentation process can favor partial SPION release, especially when the iron oxide nanocrystals are coated with hydrophilic stabilizers. This fragmentation process would probably also induce an uneven distribution of the drug, although this is not as easy to detect as for not so easy to iron nanoparticles that can be observed on cryo-TEM images. Vesicles with high SPION loading would have low encapsulation of hydrophilic drug since the available water volume will be reduced. Caricaturally, the most magnetic vesicles would not be efficient drug carriers and vice versa, reducing the utility of co-encapsulation (Figure 3). It would be highly desirable to explore the possible competitions between co-encapsulate entities more carefully.

In the case of monocompartmental systems such as nanoemulsions or SLN, SPION localization and distribution among the lipid droplets/particles constituting a given preparation have not been precisely examined so far. Nevertheless, it could be anticipated that co-encapsulation is primarily limited in these nanosystems by the intrinsic solubility of the drug in the lipids in their liquid or solid state, especially when the lipids crystallize into stable polymorphic forms [121,122]. To a certain extent, SPION encapsulation in lipophilic medium could be similarly limited. Apart from specific defavorable interactions between drug and SPION and when the concentration is below their respective solubility limits in the host lipid phase, it can be reasonably expected that drug and SPION would be randomly distributed among the nanoscale droplets or (semi)solid particles that are produced by mechanical dispersion. Nevertheless, at this stage of knowledge of these systems, it would be very informative to accurately characterize the systems to assess the actual co-encapsulation distribution profile of drug-SPION-loaded nanoemulsions or SLN.

Although eloquent results have been obtained using superparamagnetic lipid-based nanosytems in the field of pharmaceutical and biomedical applications, especially with liposomes (Table 3), some pioneering work has been dedicated to innovative strategies that could optimize the drug-SPION combination. The first group of studies aims to securely link the drug to the iron oxide nanocrystals, by a covalent or non covalent bond (Figure 4). Du et al. proposed an original thernanostic tool for multi-mechanism therapy of malignant tumors that was based on a tight but non-covalent association of the drug and SPION before their joint encapsulation within liposomes. In this system, the external surface of a C_{60}-fullerene molecule was decorated with magnetite nanoparticles and PEGylated in order to ensure its hydrophilicity and biocompatibility. The anticancer drug docetaxel was then adsorbed onto the nanoparticles, referred to as C60-Fe_3O_4-PEG_{2000} particles, and the resulting suspension was loaded into the aqueous core of DPPC-Cholesterol vesicles. The final multi-functional liposomes showed a mean hydrodynamic diameter of about 190 nm, a zeta potential of −33.6 ± 2.1 mV as well as a transverse relaxivity value (r_2) = 117 $mg.mL^{-1}.s^{-1}$ at 3 T. A study of the cytotoxicity and ability to induce apoptosis of docetaxel in these formulations confirmed that radiofrequency could remarkably improve the cellular internalization of these multi-functional liposomes and allow them to release more therapeutic agents into the cytoplasm and achieve a higher level of MCF-7 cell apoptosis *in vitro*. *In vivo*, the higher drug delivery efficiency to tumors obtained with these multi-functional liposomes localized using a magnet was striking and directly responsible for the higher tumor suppression efficacy in radiofrequency thermal therapy. An obvious darkening effect in the tumor was observed in T_2-weighted MR images of female C57 mice bearing B16-F10 tumors injected with the multi-functional liposomes with a magnet glued onto the tumor [130]. De Cuypers and his group developed « liposomes » in which individual or aggregated magnetic nanoparticles are stabilized in an aqueous medium by their entrapment in phospholipid bilayers [131]. Hodenius et al. reported the binding of 10-hydroxycamptothecin (HCPT) in the coating of these magnetoliposomes. HCPT is a chemotherapeutic anti-cancer agent, and is an example of a hydrophobic drug molecule. The mean hydrodynamic diameter of these ML

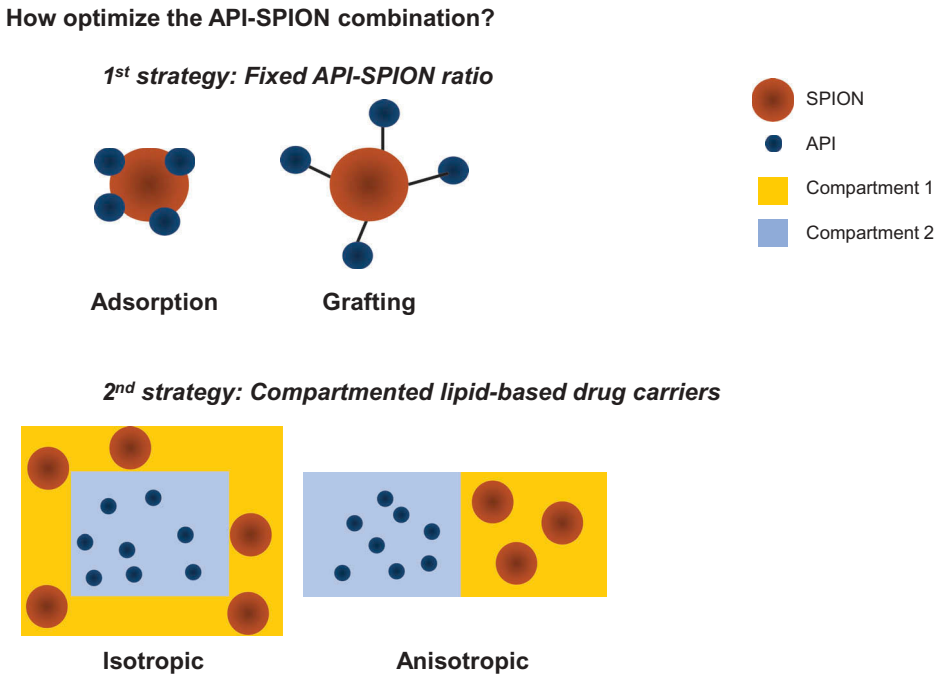

Figure 4. Proposed strategies to overcome encapsulation limitations due to competition between SPION and API.

was found to be around 91 nm and their ζ-potential was around −32.8 mV. The ML with a lipid composition DPPC/DPPG 1/3 demonstrated the highest HCPT uptake. These ML are extremely suited to carry lipophilic drugs which are practically insoluble and highly susceptible to fast deterioration in aqueous media [132]. In a similar vein, Benyettou et al. proposed original magnetoliposomes in which the drug, alendronate, is grafted onto the surface of maghemite (γ-Fe_2O_3) SPION [133]. The resulting DOPC-Cholesterol liposomes had a mean hydrodynamic diameter of 139 ± 15 nm, a ζ potential of −5 ± 3 mV. The final alendronate concentration was 400 μM and the iron oxide content was 7.2 mM. The maximum cytotoxicity of alendronate, tested on three different cell lines (breast, brain and skin tumors), was obtained only when the drug was grafted on a γ-Fe_2O_3 nanoparticle, itself included in a liposome and with a magnetic field driving force [134]. The co-localization of the SPION and the drug is guaranteed here by the covalent linkage between them.

The second strategy for the improvement of concomitant drug and SPION loading in a single lipid-based nano-object is to encapsulate the drug and the SPION in separate compartments areas to facilitate independent optimization of their respective encapsulation efficiency (Figure 4). By nature, lipid vesicles and other internally self-assembled lipid particles (ISAsomes) such as cubosomes, are delineated by lipid-based organized structures, molecular monolayers or bilayers that entrap a more or less complex network of aqueous domains. It can therefore be envisaged to incorporate the drug or the iron oxide nanocrystals separately in two distinct inner compartments. However, a limitation of nano-carriers based on mesophases formed by lyotropic lipids is that their supramolecular self-assembly can be modulated by the incorporation of exogenous entities into the supramolecular organization. These would lead to unstable bilayers or curvature problems for cubosomes [87] that could be aggravated by the particulate state of the SPION. Thus, the association of hydrophobic SPION into liposome bilayers could generate distortion of the membrane, aggregation or leakage depending on the stabilizer used [135,136]. Interestingly, the incorporation of hydrophilic SPION may cause slight alterations in bilayer fluidity levels even if it does not induce rupture or dramatic damage. Santhosh et al. point out that it is not only the concentration of SPION that affects the structural and thermodynamic properties of the membrane but the sum of factors including the number of SPION interacting with the liposomes, their size, shape and surface charge [137]. Szlezak et al. doped monoolein cubic phase with 0.2–2% (w/w) of hydrophilic (citrate) or hydrophobic (OA) SPION [138]. While no significant modification of the phase behavior was observed by adding hydrophobic nanoparticles, substantial changes in the cubic phase parameters and transition temperatures were observed with hydrophilic SPION. Moreover, this effect was more pronounced when a drug like doxorubicin is co-incorporated in the formulation. Notably, the lattice parameter increased, resulting in a reduced curvature of the bilayer. Finally, release studies from cubic phase gels (similar experiments with cubosomes are not available) clearly show significantly different doxorubicin release profiles with and without the hydrophilic SPION co-incorporated within the cubic phase. Furthermore, because of the close association between the two compartments, destabilization of one of them would destabilize the other one.

In our opinion, the next step in this field of lipid-based systems co-encapsulating SPION and drug is to design carriers

in which (1)- the encapsulation of one compound does not alter the encapsulation of the other and (2)- the interconnexion between the two compartments is as low as possible to minimize the risk of destabilization of the nano-object when one or the other is modified. Anisotropic structures with one compartment devoted to the incorporation of the SPION and another one for the drug would fit this description [139,140,141,142]. However, the development of such compartmented structures is a difficult challenge which should be addressed.

Acknowledgments

The authors gratefully acknowledge Gillian Barratt for her rereading and language revision of the manuscript.

Funding

This paper was not funded

Declaration of interest

The authors have no relevant affiliations or financial involvement with any organization or entity with a financial interest in or financial conflict with the subject matter or materials discussed in the manuscript. This includes employment, consultancies, honoraria, stock ownership or options, expert testimony, grants or patents received or pending, or royalties. Peer reviewers on this manuscript have no relevant financial or other relationships to disclose.

References

Papers of special note have been highlighted as either of interest (•) or of considerable interest (••) to readers.

1. Massart R. Preparation of aqueous magnetic liquids in alkaline and acidic media. IEEE Trans Magn. 1981;17:1247–1248.
2. Gupta AK, Gupta M. Synthesis and surface engineering of iron oxide nanoparticles for biomedical applications. Biomaterials. 2005;26:3995–4021.
3. Kostopoulou A, Lappas A. Colloidal magnetic nanocrystal clusters: variable length-scale interaction mechanisms, synergetic functionalities and technological advantages. Nanotechnol Rev [Internet]. 2015;4. [cited 2017 Apr 19]. Available from: http://www.degruyter.com/view/j/ntrev.2015.4.issue-6/ntrev-2014-0034/ntrev-2014-0034.xml
4. Belin T, Guigue-Millot N, Caillot T, et al. Influence of grain size, oxygen stoichiometry, and synthesis conditions on the γ-Fe2O3 vacancies ordering and lattice parameters. J Solid State Chem. 2002;163:459–465.
5. Gossuin Y, Gillis P, Hocq A, et al. Magnetic resonance relaxation properties of superparamagnetic particles. Wiley Interdiscip Rev Nanomed Nanobiotechnol. 2009;1:299–310.
6. Shtykova EV, Huang X, Remmes N, et al. Structure and properties of iron oxide nanoparticles encapsulated by phospholipids with poly (ethylene glycol) tails. J Phys Chem C. 2007;111:18078–18086.
7. Marie H, Plassat V, Lesieur S. Magnetic-fluid-loaded liposomes for MR imaging and therapy of cancer. J Drug Deliv Sci Technol. 2013;23:25–37.
8. Knobel M, Nunes WC, Socolovsky LM, et al. Superparamagnetism and other magnetic features in granular materials: a review on ideal and real systems. J Nanosci Nanotech. 2008;8:2836–2857.
9. Shin TH, Choi Y, Kim S, et al. Recent advances in magnetic nanoparticle-based multi-modal imaging. Chem Soc Rev. 2015;44 (14):4501–4516.
10. Bourrinet P, Bengele HH, Bonnemain B, et al. Preclinical safety and pharmacokinetic profile of ferumoxtran-10, an ultrasmall superparamagnetic iron oxide magnetic resonance contrast agent. Invest Radiol. 2006;41:313–324.
11. Leenders W. Ferumoxtran-10 advanced magnetics. IDrugs Investig Drugs J. 2003;6:987–993.
12. Bonnemain B. Superparamagnetic agents in magnetic resonance imaging: physicochemical characteristics and clinical applications a review. J Drug Target. 1998;6:167–174.
13. Reddy LH, Arias JL, Nicolas J, et al. Magnetic nanoparticles: design and characterization, toxicity and biocompatibility, pharmaceutical and biomedical applications. Chem Rev. 2012;112:5818–5878.
14. Choi HS, Liu W, Misra P, et al. Renal clearance of nanoparticles. Nat Biotechnol. 2007;25:1165–1170.
15. Veiseh O, Gunn JW, Zhang M. Design and fabrication of magnetic nanoparticles for targeted drug delivery and imaging. Adv Drug Deliv Rev. 2010;62:284–304.
16. Tanimoto A, Kuribayashi S. Application of superparamagnetic iron oxide to imaging of hepatocellular carcinoma. Eur J Radiol. 2006;58:200–216.
17. Moghimi SM. Mechanisms of splenic clearance of blood cells and particles: towards development of new splenotropic agents. Adv Drug Deliv Rev. 1995;17:103–115.
18. Roberts WG, Palade GE. Neovasculature induced by vascular endothelial growth factor is fenestrated. Cancer Res. 1997;57:765–772.
19. Matsumura Y, Maeda H. A new concept for macromolecular therapeutics in cancer chemotherapy: mechanism of tumoritropic accumulation of proteins and the antitumor agent smancs. Cancer Res. 1986;46:6387–6392.
20. Passirani C, Barratt G, Devissaguet J-P, et al. Long-circulating nanopartides bearing heparin or dextran covalently bound to poly (Methyl methacrylate). Pharm Res. 1998;15:1046–1050.
21. Anzai Y, Piccoli CW, Outwater EK, et al. evaluation of neck and body metastases to nodes with ferumoxtran 10–enhanced MR imaging: phase III safety and efficacy study. Radiology. 2003;228:777–788.
22. Chambon C, Clement O, Le Blanche A, et al. Superparamagnetic iron oxides as positive MR contrast agents: in vitro and in vivo evidence. Magn Reson Imaging. 1993;11:509–519.
23. Canet E, Revel D, Forrat R, et al. Superparamagnetic iron oxide particles and positive enhancement for myocardial perfusion studies assessed by subsecond T1-weighted MRI. Magn Reson Imaging. 1993;11:1139–1145.
24. Laurent S, Dutz S, Häfeli UO, et al. Magnetic fluid hyperthermia: focus on superparamagnetic iron oxide nanoparticles. Adv Colloid Interface Sci. 2011;166:8–23.
25. Qin J, Laurent S, Jo YS, et al. A high-Performance magnetic resonance imaging T2 contrast agent. Adv Mater. 2007;19:1874–1878.
26. Rohrer M, Bauer H, Mintorovitch J, et al. Comparison of magnetic properties of MRI contrast media solutions at different magnetic field strengths. Invest Radiol. 2005;40:715–724.
27. Xiao L, Li J, Brougham DF, et al. Water-soluble superparamagnetic magnetite nanoparticles with biocompatible coating for enhanced magnetic resonance imaging. ACS Nano. 2011;5:6315–6324.
28. Zhang K, Liang Q, Ma S, et al. On-chip manipulation of continuous picoliter-volume superparamagnetic droplets using a magnetic force. Lab Chip. 2009;9:2992.
29. Bacri J-C, Perzynski R, Salin D, et al. Magnetic colloidal properties of ionic ferrofluids. J Magn Magn Mater. 1986;62:36–46.
30. Tan MC. Nanostructured materials for biomedical applications. Kerala: Transworld research network; 2009.
31. Voit W, Kim DK, Zapka W, et al. Magnetic behavior of coated superparamagnetic iron oxide nanoparticles in ferrofluids. MRS Online Proc Libr Arch [Internet]. 2001;676. cited 2016 Dec 7. Available from: https://www.cambridge.org/core/journals/mrs-online-proceedings-library-archive/article/magnetic-behavior-of-coated-superparamagnetic-iron-oxide-nanoparticles-in-ferrofluids/773F77C91B3DA675523D62C5E675E576
32. Yang J, Lee H, Hyung W, et al. Magnetic PECA nanoparticles as drug carriers for targeted delivery: synthesis and release characteristics. J Microencapsul. 2006;23:203–212.

33. Huang Y, Mao K, Zhang B, et al. Superparamagnetic iron oxide nanoparticles conjugated with folic acid for dual target-specific drug delivery and MRI in cancer theranostics. Mater Sci Eng C. 2017;70(Part 1):763–771.
34. Kim D-H, Lee S-H, Kim K-N, et al. Temperature change of various ferrite particles with alternating magnetic field for hyperthermic application. J Magn Magn Mater. 2005;293:320–327.
35. Wang X, Gu H, Yang Z. The heating effect of magnetic fluids in an alternating magnetic field. J Magn Magn Mater. 2005;293:334–340.
36. Shellman YG, Howe WR, Miller LA, et al. Hyperthermia induces endoplasmic reticulum-mediated apoptosis in melanoma and non-melanoma skin cancer cells. J Invest Dermatol. 2008;128:949–956.
37. Hildebrandt B, Wust P, Ahlers O, et al. The cellular and molecular basis of hyperthermia. Crit Rev Oncol Hematol. 2002;43:33–56.
38. Wust P, Hildebrandt B, Sreenivasa G, et al. Hyperthermia in combined treatment of cancer. Lancet Oncol. 2002;3:487–497.
39. Brusentsov NA, Brusentsova TN, Sergeev AV, et al. Ferrimagnetic fluids and ferro-and ferrimagnetic suspensions for the RF-induction hyperthermia of tumors. Pharm Chem J. 2000;34:201–207.
40. Matsuoka F, Shinkai M, Honda H, et al. Hyperthermia using magnetite cationic liposomes for hamster osteosarcoma. Biomagn Res Technol. 2004;2:1.
41. Kikumori T, Kobayashi T, Sawaki M, et al. Anti-cancer effect of hyperthermia on breast cancer by magnetite nanoparticle-loaded anti-HER2 immunoliposomes. Breast Cancer Res Treat. 2009;113:435.
42. Same S, Aghanejad A, Akbari Nakhjavani S, et al. Radiolabeled theranostics: magnetic and gold nanoparticles. Bioimpacts. 2016;6:169–181.
43. Kievit FM, Zhang M. Surface engineering of iron oxide nanoparticles for targeted cancer therapy. Acc Chem Res. 2011;44:853–862.
44. Thomas R, Park I-K, Jeong Y. Magnetic iron oxide nanoparticles for multimodal imaging and therapy of cancer. Int J Mol Sci. 2013;14:15910–15930.
45. Laurent S, Saei AA, Behzadi S, et al. Superparamagnetic iron oxide nanoparticles for delivery of therapeutic agents: opportunities and challenges. Expert Opin Drug Deliv. 2014;11:1449–1470.
46. Hauss DJ. Oral lipid-based formulations. Enhancing the bioavailability of poorly water soluble drugs. Boca Rato, FL: CRC press, Taylor and Francis Group; 2007.
47. Bangham AD, Standish MM, Watkins JC. Diffusion of univalent ions across the lamellae of swollen phospholipids. J Mol Biol. 1965;13:238–IN27.
48. Li G, Zhou Z, Li Y, et al. Surface functionalization of chitosan-coated magnetic nanoparticles for covalent immobilization of yeast alcohol dehydrogenase from Saccharomyces cerevisiae. J Magn Magn Mater. 2010;322:3862–3868.
49. Zhang Y, Liu J-Y, Ma S, et al. Synthesis of PVP-coated ultra-small Fe3O4 nanoparticles as a MRI contrast agent. J Mater Sci Mater Med. 2010;21:1205–1210.
50. Harisinghani M, Ross RW, Guimaraes AR, et al. Utility of a new bolus-injectable nanoparticle for clinical cancer staging. Neoplasia. 2007;9:1160–1165.
51. Mahmoudi M, Simchi A, Imani M, et al. Optimal design and characterization of superparamagnetic iron oxide nanoparticles coated with polyvinyl alcohol for targeted delivery and imaging †. J Phys Chem B. 2008;112:14470–14481.
52. Carvalho A, Martins MBF, Corvo ML, et al. Enhanced contrast efficiency in MRI by PEGylated magnetoliposomes loaded with PEGylated SPION: effect of SPION coating and micro-environment. Mater Sci Eng C. 2014;43:521–526.
53. Ma H, Qi X, Maitani Y, et al. Preparation and characterization of superparamagnetic iron oxide nanoparticles stabilized by alginate. Int J Pharm. 2007;333:177–186.
54. Fattahi H, Laurent S, Liu F, et al. Magnetoliposomes as multimodal contrast agents for molecular imaging and cancer nanotheragnostics. Nanomed. 2011;6:529–544.
55. Monnier CA, Burnand D, Rothen-Rutishauser B, et al. Magnetoliposomes: opportunities and challenges. Eur J Nanomedicine [Internet]. 2014;6. cited 2017 May 19. Available from: https://www.degruyter.com/view/j/ejnm.2014.6.issue-4/ejnm-2014-0042/ejnm-2014-0042.xml
56. Soenen SJ, Velde GV, Ketkar-Atre A, et al. Magnetoliposomes as magnetic resonance imaging contrast agents. Wiley Interdiscip Rev Nanomed Nanobiotechnol. 2011;3:197–211.
57. Ji B, Wang M, Gao D, et al. Combining nanoscale magnetic nimodipine liposomes with magnetic resonance image for Parkinson's disease targeting therapy. Nanomed. 2017;12:237–253.
58. Martina M-S, Fortin J-P, Ménager C, et al. Generation of superparamagnetic liposomes revealed as highly efficient MRI contrast agents for in vivo imaging. J Am Chem Soc. 2005;127:10676–10685.
59. Plassat V, Martina MS, Barratt G, et al. Sterically stabilized superparamagnetic liposomes for MR imaging and cancer therapy: pharmacokinetics and biodistribution. Int J Pharm. 2007;344:118–127.
60. Marie H, Lemaire L, Franconi F, et al. Superparamagnetic liposomes for MRI monitoring and external magnetic field-induced selective targeting of malignant brain tumors. Adv Funct Mater. 2015;25:1258–1269.
61. Plassat V, Wilhelm C, Marsaud V, et al. Anti-estrogen-loaded superparamagnetic liposomes for intracellular magnetic targeting and treatment of breast cancer tumors. Adv Funct Mater. 2011;21:83–92.
62. Ye H, Tong J, Liu J, et al. Combination of gemcitabine-containing magnetoliposome and Oxaliplatin-containing magnetoliposomes in breast cancer treatment: a possible mechanism with potential for clinical application. Oncotarget. 2016;7:43762–43778.
63. Viroonchatapan E, Sato H, Ueno M, et al. Release of 5-fluorouracil from thermosensitive magnetoliposomes induced by an electromagnetic field. J Controlled Release. 1997;46:263–271.
64. Yoshida M, Watanabe Y, Sato M, et al. Feasibility of chemohyperthermia with docetaxel-embedded magnetoliposomes as minimally invasive local treatment for cancer. Int J Cancer. 2010;126:1955–1965.
65. Yoshida M, Sato M, Yamamoto Y, et al. Tumor local chemohyperthermia using docetaxel-embedded magnetoliposomes: interaction of chemotherapy and hyperthermia. J Gastroenterol Hepatol. 2012;27:406–411.
66. Bolfarini GC, Siqueira-Moura MP, Demets GJF, et al. In vitro evaluation of combined hyperthermia and photodynamic effects using magnetoliposomes loaded with cucurbit[7]uril zinc phthalocyanine complex on melanoma. J Photochem Photobiol B. 2012;115:1–4.
67. Di Corato R, Béalle G, Kolosnjaj-Tabi J, et al. Combining magnetic hyperthermia and photodynamic therapy for tumor ablation with photoresponsive magnetic liposomes. ACS Nano. 2015;9:2904–2916.
68. Ferreira RV, Martins TM, Goes AM, et al. Thermosensitive gemcitabine-magnetoliposomes for combined hyperthermia and chemotherapy. Nanotechnology. 2016;27:085105.
69. Kulshrestha P, Gogoi M, Bahadur D, et al. In vitro application of paclitaxel loaded magnetoliposomes for combined chemotherapy and hyperthermia. Colloids Surf B Biointerfaces. 2012;96:1–7.
70. Clares B, Biedma-Ortiz RA, Sáez-Fernández E, et al. Nano-engineering of 5-fluorouracil-loaded magnetoliposomes for combined hyperthermia and chemotherapy against colon cancer. Eur J Pharm Biopharm. 2013;85:329–338.
71. Chen Y, Chen Y, Xiao D, et al. Low-dose chemotherapy of hepatocellular carcinoma through triggered-release from bilayer-decorated magnetoliposomes. Colloids Surf B Biointerfaces. 2014;116:452–458.
72. Bothun GD, Lelis A, Chen Y, et al. Multicomponent folate-targeted magnetoliposomes: design, characterization, and cellular uptake. Nanomedicine Nanotechnol Biol Med. 2011;7:797–805.
73. Sharma S, Rasool HI, Palanisamy V, et al. Structural-mechanical characterization of nanoparticle exosomes in human saliva, using correlative AFM, FESEM, and force spectroscopy. ACS Nano. 2010;4:1921–1926.

74. Ha D, Yang N, Nadithe V. Exosomes as therapeutic drug carriers and delivery vehicles across biological membranes: current perspectives and future challenges. Acta Pharm Sin B. 2016;6:287–296.
75. Sun D, Zhuang X, Zhang S, et al. Exosomes are endogenous nanoparticles that can deliver biological information between cells. Adv Drug Deliv Rev. 2013;65:342–347.
76. Hood JL, Scott MJ, Wickline SA. Maximizing exosome colloidal stability following electroporation. Anal Biochem. 2014;448:41–49.
77. Hu L, Wickline SA, Hood JL. Magnetic resonance imaging of melanoma exosomes in lymph nodes. Magn Reson Med. 2015;74:266–271.
78. Chung T-H, Hsiao J-K, Yao M, et al. Ferucarbotran, a carboxydextran-coated superparamagnetic iron oxide nanoparticle, induces endosomal recycling, contributing to cellular and exosomal EGFR overexpression for cancer therapy. RSC Adv. 2015;5:89932–89939.
79. Silva AKA, Luciani N, Gazeau F, et al. Combining magnetic nanoparticles with cell derived microvesicles for drug loading and targeting. Nanomedicine Nanotechnol Biol Med. 2015;11:645–655.
• **A thorough *in vitro* work on microvesicles**
80. Qi H, Liu C, Long L, et al. Blood exosomes endowed with magnetic and targeting properties for cancer therapy. ACS Nano. 2016;10:3323–3333.
•• **A promising work in the new field of exosomes.**
81. Piffoux M, Silva AKA, Lugagne J-B, et al. Extracellular vesicle production loaded with nanoparticles and drugs in a trade-off between loading, yield and purity: towards a personalized drug delivery system. Adv Biosyst. 2017;1:1700044.
82. Stroem P, Anderson DM. The cubic phase region in the system didodecyldimethylammonium bromide-water-styrene. Langmuir. 1992;8:691–709.
83. Lynch ML, Kochvar KA, Burns JL, et al. Aqueous-phase behavior and cubic phase-containing emulsions in the $C_{12}E_2$–Water System. Langmuir. 2000;16:3537–3542.
84. Nanjwade BK, Hundekar YR, Kamble MS, et al. Development of cuboidal nanomedicine by nanotechnology. Austin J Nanomed Nanotechnol. 2014;2:1023.
85. Garg G, Saraf S, Saraf S. Cubosomes: an overview. Biol Pharm Bull. 2007;30:350–353.
86. Drummond CJ, Fong C. Surfactant self-assembly objects as novel drug delivery vehicles. Curr Opin Colloid Interface Sci. 1999;4:449–456.
87. Acharya DP, Moffat BA, Polyzos A, et al. Cubic mesophase nanoparticles doped with superparamagnetic iron oxide nanoparticles: a new class of MRI contrast agent. RSC Adv. 2012;2:6655–6662.
88. Montis C, Castroflorio B, Mendozza M, et al. Magnetocubosomes for the delivery and controlled release of therapeutics. J Colloid Interface Sci. 2015;449:317–326.
89. Hong SK, Ma JY, Kim J-C. Preparation of iron oxide nanoparticles within monoolein cubic phase. J Ind Eng Chem. 2012;18:1977–1982.
90. Wang MH, Kim J-C. Magnetic field-responsive cubosomes containing magnetite and poly(N-isopropylacrylamide). J Controlled Release. 2013;172:e139.
• **An original way to control the drug release from cubosomes with a thermosensitive polymer in response to hyperthermia induced by SPION.**
91. Gupta A, Eral HB, Hatton TA, et al. Nanoemulsions: formation, properties and applications. Soft Matter. 2016;12:2826–2841.
92. Singh Y, Meher JG, Raval K, et al. Nanoemulsion: concepts, development and applications in drug delivery. J Controlled Release. 2017;252:28–49.
93. Salcido A. Equilibrium properties of the cellular automata models for traffic flow in a single lane. In: Salcido A, editor. Cell autom - Simplicity Complex [Internet]. InTech; 2011. [cited 2017 May 19]. Rijeka, Croatia. Available from: http://www.intechopen.com/books/cellular-automata-simplicity-behind-complexity/equilibrium-properties-of-the-cellular-automata-models-for-traffic-flow-in-a-single-lane
94. Bates TR, Carrigan PJ. Apparent absorption kinetics of micronized griseofulvin after its oral administration on single- and multiple-dose regimens to rats as a corn oil-in-water emulsion and aqueous suspension. J Pharm Sci. 1975;64:1475–1481.
95. Sainsbury F, Zeng B, Middelberg AP. Towards designer nanoemulsions for precision delivery of therapeutics. Curr Opin Chem Eng. 2014;4:11–17.
96. Ganta S, Amiji M. Coadministration of paclitaxel and curcumin in nanoemulsion formulations to overcome multidrug resistance in tumor cells. Mol Pharm. 2009;6:928–939.
97. Kretzer IF, Maria DA, Maranhão RC. Drug-targeting in combined cancer chemotherapy: tumor growth inhibition in mice by association of paclitaxel and etoposide with a cholesterol-rich nanoemulsion. Cell Oncol. 2012;35:451–460.
98. Chuan YP, Zeng BY, O'Sullivan B, et al. Co-delivery of antigen and a lipophilic anti-inflammatory drug to cells via a tailorable nanocarrier emulsion. J Colloid Interface Sci. 2012;368:616–624.
99. Song Y-C, Cheng H-Y, Leng C-H, et al. A novel emulsion-type adjuvant containing CpG oligodeoxynucleotides enhances CD8+ T-cell-mediated anti-tumor immunity. J Controlled Release. 2014;173:158–165.
100. Sadurní N, Solans C, Azemar N, et al. Studies on the formation of O/W nano-emulsions, by low-energy emulsification methods, suitable for pharmaceutical applications. Eur J Pharm Sci. 2005;26:438–445.
101. Lan Q, Liu C, Yang F, et al. Synthesis of bilayer oleic acid-coated Fe3O4 nanoparticles and their application in pH-responsive Pickering emulsions. J Colloid Interface Sci. 2007;310:260–269.
102. Bloemen M, Brullot W, Luong TT, et al. Improved functionalization of oleic acid-coated iron oxide nanoparticles for biomedical applications. J Nanoparticle Res. 2012;14:1–10.
103. Zhang L, He R, Gu H-C. Oleic acid coating on the monodisperse magnetite nanoparticles. Appl Surf Sci. 2006;253:2611–2617.
104. Ramella D, Polito L, Mazzini S, et al. A strategy for multivalent presentation of carba analogues from N. meningitidis a capsular polysaccharide. Eur J Org Chem. 2014;2014:5915–5924.
105. Lartigue L, Oumzil K, Guari Y, et al. Water-soluble rhamnose-coated Fe_3O_4 nanoparticles. Org Lett. 2009;11:2992–2995.
106. Lu C, Bhatt LR, Jun HY, et al. Carboxyl–polyethylene glycol–phosphoric acid: a ligand for highly stabilized iron oxide nanoparticles. J Mater Chem. 2012;22:19806.
107. White MA, Johnson JA, Koberstein JT, et al. Toward the syntheses of universal ligands for metal oxide surfaces: controlling surface functionality through click chemistry. J Am Chem Soc. 2006;128:11356–11357.
108. Liang S, Wang Y, Yu J, et al. Surface modified superparamagnetic iron oxide nanoparticles: as a new carrier for bio-magnetically targeted therapy. J Mater Sci Mater Med. 2007;18:2297–2302.
109. Koh I, Wang X, Varughese B, et al. Magnetic iron oxide nanoparticles for biorecognition: evaluation of surface coverage and activity. J Phys Chem B. 2006;110:1553–1558.
110. Zhang C, Wängler B, Morgenstern B, et al. Silica- and alkoxysilane-coated ultrasmall superparamagnetic iron oxide particles: a promising tool to label cells for magnetic resonance imaging. Langmuir. 2007;23:1427–1434.
111. Alwi R, Telenkov S, Mandelis A, et al. Silica-coated super paramagnetic iron oxide nanoparticles (SPION) as biocompatible contrast agent in biomedical photoacoustics. Biomed Opt Express. 2012;3:2500–2509.
112. Jarzyna PA, Skajaa T, Gianella A, et al. Iron oxide core oil-in-water emulsions as a multifunctional nanoparticle platform for tumor targeting and imaging. Biomaterials. 2009;30:6947–6954.
113. Deddens LH, Jarzyna PA, Griffioen AW, et al. RGD-Functionalized Superparamagnetic Nanoemulsions for Target-Specific Imaging of Tumor Angiogenesis. [cited 2016 Jun 30]. Available from: http://cds.ismrm.org/protected/10MProceedings/files/3749_1153.pdf.
114. Gianella A, Jarzyna PA, Mani V, et al. Multifunctional nanoemulsion platform for imaging guided therapy evaluated in experimental cancer. ACS Nano. 2011;5:4422–4433.
•• **Through several papers, this group has built nanoemulsions with multiple functions as drug carriers, MRI and fluorescence imaging and targeting.**
115. Manjunath K, Venkateswarlu V. Pharmacokinetics, tissue distribution and bioavailability of clozapine solid lipid nanoparticles after

intravenous and intraduodenal administration. J Controlled Release. 2005;107:215–228.
116. Varshosaz J, Tabbakhian M, Mohammadi MY. Formulation and optimization of solid lipid nanoparticles of buspirone HCl for enhancement of its oral bioavailability. J Liposome Res. 2010;20:286–296.
117. Sarmento B, Martins S, Ferreira D, et al. Oral insulin delivery by means of solid lipid nanoparticles. Int J Nanomedicine. 2007;2:743.
118. Yang R, Gao R, Li F, et al. The influence of lipid characteristics on the formation, in vitro release, and in vivo absorption of protein-loaded SLN prepared by the double emulsion process. Drug Dev Ind Pharm. 2011;37:139–148.
119. Luo Y, Chen D, Ren L, et al. Solid lipid nanoparticles for enhancing vinpocetine's oral bioavailability. J Controlled Release. 2006;114:53–59.
120. Chen -C-C, Tsai T-H, Huang Z-R, et al. Effects of lipophilic emulsifiers on the oral administration of lovastatin from nanostructured lipid carriers: physicochemical characterization and pharmacokinetics. Eur J Pharm Biopharm. 2010;74:474–482.
121. Müller RH, Runge SA, Ravelli V, et al. Cyclosporine-loaded solid lipid nanoparticles (SLN®): drug–lipid physicochemical interactions and characterization of drug incorporation. Eur J Pharm Biopharm. 2008;68:535–544.
122. Müller RH, Maaβen S, Weyhers H, et al. Cytotoxicity of magnetite-loaded polylactide, polylactide/glycolide particles and solid lipid nanoparticles. Int J Pharm. 1996;138:85–94.
123. Grillone A, Riva ER, Mondini A, et al. Active targeting of sorafenib: preparation, characterization, and in vitro testing of drug-loaded magnetic solid lipid nanoparticles. Adv Healthc Mater. 2015;4:1681–1690.
124. Zhao S, Zhang Y, Han Y, et al. Preparation and characterization of cisplatin Magnetic Solid Lipid Nanoparticles (MSLNs): effects of loading procedures of Fe3O4 nanoparticles. Pharm Res. 2014;32:482–491.
125. Oumzil K, Ramin MA, Lorenzato C, et al. Solid lipid nanoparticles for image-guided therapy of atherosclerosis. Bioconjug Chem. 2016;27:569–575.
126. Pang X, Cui F, Tian J, et al. Preparation and characterization of magnetic solid lipid nanoparticles loaded with ibuprofen. Asian J Pharm Sci. 2009;4:132–137.
127. Ying X-Y, Du Y-Z, Hong L-H, et al. Magnetic lipid nanoparticles loading doxorubicin for intracellular delivery: preparation and characteristics. J Magn Magn Mater. 2011;323:1088–1093.
128. Hsu M-H, Su Y-C. Iron-oxide embedded solid lipid nanoparticles for magnetically controlled heating and drug delivery. Biomed Microdevices. 2008;10:785–793.
129. Albuquerque J, Moura C, Sarmento B, et al. Solid lipid nanoparticles: a potential multifunctional approach towards rheumatoid arthritis theranostics. Molecules. 2015;20:11103–11118.
130. Du B, Han S, Li H, et al. Multi-functional liposomes showing radiofrequency-triggered release and magnetic resonance imaging for tumor multi-mechanism therapy. Nanoscale. 2015;7:5411–5426.
131. De Cuyper M, Joniau M. Magnetoliposomes. Eur Biophys J. 1988;15:311–319.
132. Hodenius MAJ, Schmitz-Rode T, Baumann M, et al. Absorption of 10-hydroxycamptothecin into the coat of magnetoliposomes. Colloids Surf Physicochem Eng Asp. 2009;343:20–23.
133. Benyettou F, Guenin E, Lalatonne Y, et al. Microwave assisted nanoparticle surface functionalization. Nanotechnology. 2011;22:055102.
134. Benyettou F, Chebbi I, Motte L, et al. Magnetoliposome for alendronate delivery. J Mater Chem. 2011;21:4813–4820.
135. Amstad E, Kohlbrecher J, Müller E, et al. Triggered release from liposomes through magnetic actuation of iron oxide nanoparticle containing membranes. Nano Lett. 2011;11:1664–1670.
• **Interesting investigation and discussion on the incorporation of SPION into phospholipid bilayers.**
136. Chen Y, Bose A, Bothun GD. Controlled release from bilayer-decorated magnetoliposomes via electromagnetic heating. ACS Nano. 2010;4:3215–3221.
137. Budime Santhosh P, Drasler B, Drobne D, et al. Effect of superparamagnetic iron oxide nanoparticles on fluidity and phase transition of phosphatidylcholine liposomal membranes. Int J Nanomedicine. 2015;10: 6089–6104.
138. Szlezak M, Nieciecka D, Joniec A, et al. Monoolein cubic phase gels and cubosomes doped with magnetic nanoparticles–hybrid materials for controlled drug release. ACS Appl Mater Interfaces. 2017;9:2796–2805.
• **Deep and well-conducted studies on the interactions between hydrophylic or hydrophobic SPION and cubic phases.**
139. Tran L-T-C, Lesieur S, Faivre V. Janus nanoparticles: materials, preparation and recent advances in drug delivery. Expert Opin Drug Deliv. 2014;11:1061–1074.
140. Bonnaud C, Monnier CA, Demurtas D, et al. Insertion of nanoparticle clusters into vesicle bilayers. ACS Nano. 2014;8:3451–3460.
141. Walther A, Müller AHE. Janus particles: synthesis, self-assembly, physical properties, and applications. Chem Rev. 2013;113:5194–5261.
142. Truong-Cong T, Millart E, Tran L-T-C, et al. Nanoscale. 2018;10:3654–3662.